

# Underwater Detection and Communication Integrated Waveform Design Based on P4 Encoding

Qixiang Niu<sup>a,b</sup>, David Ramírez<sup>b,c</sup>, Wentao Shi<sup>a,d,\*</sup>, and Qunfei Zhang<sup>a</sup>

<sup>a</sup> School of Marine Science and Technology, Northwestern Polytechnical University, Xi'an, 710072, China

<sup>b</sup> Department of Signal Theory and Communications, Universidad Carlos III de Madrid, Leganés, 28911, Spain

<sup>c</sup> Instituto de Investigación Sanitaria Gregorio Marañón, Madrid, 28009, Spain

<sup>d</sup> Ocean Institute, Northwestern Polytechnical University, Taicang, 215400, China

\* Email: swt@nwpu.edu.cn

**Abstract**—Affine Frequency Division Multiplexing (AFDM) has emerged as a promising waveform for integrated underwater detection and communication (IUDC) due to its low computational complexity and robust sensing capabilities. This paper investigates AFDM-based underwater systems, focusing on the impact of signal coding on detection performance through the discrete wideband ambiguity function (WAF). An enhanced P4 coding scheme is proposed, incorporating random phase perturbations optimized via particle swarm optimization (PSO) to improve the WAF properties. The proposed method effectively enhances detection performance by significantly reducing sidelobe levels compared to conventional P4 coding, as demonstrated through simulations. Furthermore, the approach maintains reliable communication with minimal bit error rate degradation. By adjusting the maximum phase perturbation, the method offers a flexible trade-off between detection and communication performance, providing a robust and efficient solution for underwater sensing and data transmission.

**Index Terms**—AFDM, ambiguity function, integrated underwater detection and communication (IUDC), P4 coding, random phase perturbation.

## I. INTRODUCTION

Integrated sensing and communication (ISAC) has emerged as a pivotal technology in next-generation wireless communication systems, enabling resource sharing on a single hardware platform to significantly enhance spectral efficiency and reduce hardware costs. In aerial wireless environments, ISAC supports both efficient communication and high-precision sensing. However, underwater ISAC systems face unique challenges, including limited bandwidth, power constraints, and real-time processing capabilities, complicating the coordination of data transmission and target detection. The underwater acoustic environment further introduces severe multipath effects, time-varying channels, high propagation loss, and Doppler spread, limiting the application of ISAC technologies in these settings. Consequently, ISAC remains in an early exploratory stage for underwater use and is not yet well integrated with integrated underwater detection and communication (IUDC) [1].

The primary challenge of IUDC lies in achieving both high-precision sensing and efficient communication in doubly selective underwater channels while overcoming technical barriers related to signal design, channel estimation, and inter-

ference suppression. Addressing these challenges is essential for advancing IUDC, which holds significant potential for applications such as ocean resource exploration, underwater robotics, submarine navigation, and marine environmental monitoring. Overcoming these challenges requires advanced waveform design and joint sensing-communication processing to lay a solid foundation for IUDC deployment [2].

Recently, scholars have explored the discrete affine Fourier transform (DAFT) as the foundation of affine frequency division multiplexing (AFDM). AFDM is designed to overcome the limitations of traditional waveforms like orthogonal frequency division multiplexing (OFDM) and orthogonal time-frequency space (OTFS) in complex environments, including high-mobility scenarios and doubly dispersive underwater channels [3]. Studies show that AFDM achieves comparable bit error rate (BER) performance to OTFS while offering lower complexity and reduced channel pilot overhead. A sparse code multiple access system based on AFDM has also been proposed, with experimental results demonstrating its significant performance gains over OFDM in both uncoded and coded systems.

Despite its advantages, AFDM has certain limitations. Its reliance on time-frequency modulation makes it susceptible to channel estimation errors and multipath interference. Additionally, traditional AFDM demodulation is highly sensitive to the dynamic nature of underwater channels, leading to significant degradation in detection performance under rapidly varying conditions [4]. Addressing these challenges necessitates advancements in coding algorithms to enhance AFDM's robustness against noise, multipath effects, and dynamic channel variations. Such improvements are essential for achieving reliable and efficient IUDC in complex underwater environments [5].

Recent research on coding techniques has focused on improving ISAC waveform design. For instance, turbo coding enhances communication reliability and noise resistance, while polar coding reduces error rates and improves radar robustness [6]. Adaptive coding that adjusts parameters based on channel conditions and compressed sensing-based coding that leverages signal sparsity to reduce complexity and energy consumption also show great potential. These advances

have improved signal detection and communication in ISAC systems and are expected to yield similar benefits in IUDC [7].

This work enhances AFDM signal detection in underwater environments through advanced coding techniques. We analyze the wideband ambiguity function (WAF) to assess its impact on AFDM and propose coding improvements that suppress sidelobes, thereby enhancing detection capabilities. Using phase four (P4) coding [8] as a baseline, we introduce random perturbations, where "random phase perturbation" in this context means that it is not related to improving communication performance and is unknown at the receiver optimized via a particle swarm optimization (PSO) algorithm to improve the WAF properties. Detection performance is evaluated before and after this enhancement, demonstrating its effectiveness.

## II. SYSTEM MODEL

Fig. 1 illustrates the overall architecture of the IUDC system. The diagram shows the system's integrated structure, including the processes of target detection and echo retrieval. The detection signal emitted by the sonar transducer interacts with multiple targets, generating corresponding echoes that, once processed, yield both sensing and communication information. This integrated waveform design approach not only enhances underwater localization accuracy but also enables efficient communication in complex underwater environments. Therefore, designing a waveform suitable for the IUDC system is of paramount importance, and the content of this chapter is developed accordingly.

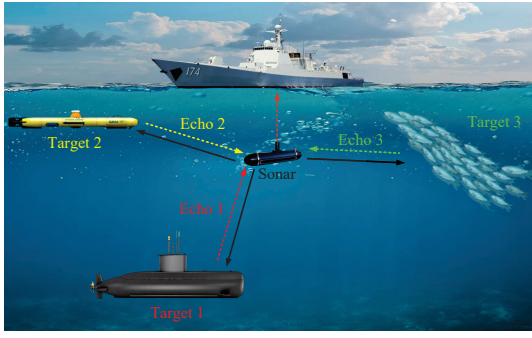


Fig. 1. An integrated underwater detection and communication system using sonar transmission and echo reception

### A. AFDM-based discrete WAF model

This section begins with the modeling of the discrete wideband ambiguity function (WAF), which characterizes the time delay and Doppler characteristics of wideband signals. In underwater environments, where acoustic wave propagation is slow and target motion induces significant Doppler effects, the WAF proves highly effective in studying frequency-dependent effects. Moreover, wideband signals offer enhanced range and velocity resolution, making them ideal for complex

underwater environments with significant noise and multipath propagation [9], [10]. The WAF of  $s(t)$  is given by

$$\psi_{\text{WAF}}(\tau, \alpha) = |\chi(\tau, \alpha)|^2 = \left| \sqrt{\alpha} \int_{-\infty}^{\infty} s(t)s^*(\alpha(t - \tau)) dt \right|^2, \quad (1)$$

where  $\alpha = \frac{c-v_m}{c+v_m}$  denotes the Doppler scaling factor, with  $c$  representing the underwater sound speed and  $v_m$  the radial velocity. It is possible to discretize (1) as

$$\psi_{\text{WAF}}[m, \beta] = \left| \sqrt{\alpha_\beta} \sum_{k=-\infty}^{\infty} s[k]s^*[\alpha_\beta(k-m)] \right|^2, \quad (2)$$

where  $s[k]$  denotes the transmitted (discrete) signal and  $m$  the time delay. The Doppler scaling factor,  $\alpha_\beta$ , is defined as  $\alpha_\beta = 1 + \frac{\beta}{N}$ , where  $N$  is the signal length and  $\beta$  the Doppler frequency shift index. If  $\alpha_\beta$  is non-integer, we can use signal interpolation to evaluate (2). The term  $s^*[\alpha_\beta(k-m)]$  represents the complex conjugate of the signal, incorporating both time delay and Doppler scaling.

The modulation model of AFDM is introduced next. In the DAFT domain, let  $x[n], n = 0, 1, \dots, N-1$ , represent the communication symbol carried by each subcarrier, where  $N$  is the total number of subcarriers. The AFDM transmitter applies an inverse DAFT (IDAFT) with parameters  $(c_1, c_2)$ , where  $c_1$  determines the chirp slope and  $c_2$  is an additional system parameter. The IDAFT is given by

$$s[k] = \frac{1}{\sqrt{N}} \sum_{n=0}^{N-1} x[n] \exp \left( j2\pi \left( c_2 n^2 + \frac{1}{N} nk + c_1 k^2 \right) \right). \quad (3)$$

Substituting (3) into (2), the WAF of the AFDM signal is

$$\psi_{\text{WAF}}[m, \beta] = \frac{\alpha_\beta}{N^2} \left| \sum_{k=0}^{N-1} \sum_{i,p=0}^{N-1} x[i]x^*[p] \exp(j2\pi\gamma(k, i, p, m, \beta)) \right|^2, \quad (4)$$

where

$$\begin{aligned} \gamma(k, i, p, m, \beta) &= c_2 i^2 + \frac{ik}{N} + c_1 k^2 \\ &- \left( c_2 p^2 + \frac{p \cdot \alpha_\beta(k-m)}{N} + c_1 (\alpha_\beta(k-m))^2 \right). \end{aligned} \quad (5)$$

The WAF in (4) shows that  $x[n]$ , the symbol sequence, determines the WAF. Thus, it can be used for the coding optimization, discussed later, that aims to enhance the IUDC detection performance of AFDM signals.

### B. Underwater multipath fading channel model

In this study, the underwater channel is modeled as a multipath fading channel using the Jakes sinusoidal superposition method [11]. The transfer function of this multipath fading channel is

$$H(t) = H_r(t) + jH_q(t), \quad (6)$$

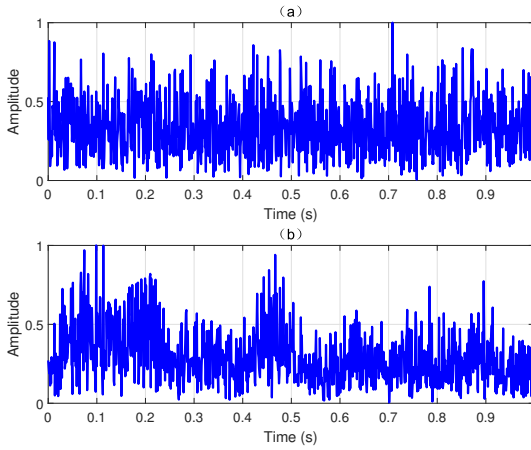


Fig. 2. Comparison of the AFDM waveform with P4 coding through the Jakes-model multipath fading channel: (a) before the channel; (b) after the multipath fading channel

where

$$H_r(t) = \sqrt{2} \cos \phi_M \cos \omega_d t + 2 \sum_{m=1}^{M_0} \cos \phi_m \cos \omega_m t, \quad (7)$$

and

$$H_q(t) = \sqrt{2} \sin \phi_M \cos \omega_d t + 2 \sum_{m=1}^{M_0} \sin \phi_m \cos \omega_m t. \quad (8)$$

Here,  $M_0$  denotes the number of sinusoidal components used to model Doppler shifts, which must be sufficiently large to achieve an accurate Rayleigh amplitude approximation. In this study, we set  $M_0 = 32$ . The initial phase is represented by  $\phi_M$ , while the phase of each component is given by  $\phi_m = \frac{m\pi}{M_0+1}$ . The initial angular frequency is defined as  $\omega_d = 2\pi f_c$ , where  $f_c$  is the carrier frequency. The angular frequency of each component is expressed as  $\omega_m = \omega_d \cos(\frac{2\pi m}{M})$ . A realization of  $|H(t)|$  is illustrated in Fig. 2.

### III. OPTIMIZED RANDOM PERTURBATION P4 CODING ALGORITHM

P4 encoding, or the fourth polyphase code, is a specialized sequence originally designed for radar and communication due to its excellent autocorrelation and anti-interference properties [12]. With strong Doppler tolerance and low cross-correlation, it is highly suited for ISAC applications. By employing a structured phase design to suppress signal sidelobes, P4 encoding enhances resolution and interference resistance, offering significant advantages for integrated sensing and communication systems. The phase of the  $n$ -th element in P4 encoding is given by:

$$\phi[n] = \pi \cdot \frac{n^2}{N} - \pi n, \quad n = 0, 1, \dots, N-1. \quad (9)$$

The corresponding complex signal can be expressed as follows, where:

$$x[n] = e^{j\phi_n} = e^{j(\pi \frac{n^2}{N} - \pi n)}, \quad (10)$$

where  $N$  is the length of the encoding sequence, and  $\phi_n$  represents the phase of the  $n$ -th signal.

Although P4 coding exhibits excellent autocorrelation, underwater multipath conditions can significantly raise its peak sidelobe level (PSL), which reduces detection accuracy. Additionally, Doppler shifts distort its phase characteristics, degrading sensing performance and communication reliability. To counter this, phase adjustments can suppress sidelobe amplitudes, maintaining low autocorrelation sidelobes even under multipath conditions, thereby enhancing target detection accuracy.

In the DAFT domain, we propose to perturb the symbols as

$$x'[n] = x[n] \cdot e^{j(\phi[n] + \theta[n])}, \quad n = 0, 1, \dots, N-1, \quad (11)$$

where  $\theta[n]$  is the random phase perturbation. By adjusting  $\boldsymbol{\theta} = [\theta[0], \dots, \theta[N-1]]^T$ , PSL interference can be minimized. Since this adjustment is interpreted as noise during reception, no changes to the IUDC receiver's processing system are required.

While allowing for larger phase perturbations can further reduce the PSL of the AFDM signal, it also leads to an increase in the bit error rate [13]. Therefore, the phase perturbation must be constrained within a maximum allowable value,  $\theta_{\max}$ . Then,  $\boldsymbol{\theta}$  is obtained by minimizing the PSL while adhering to the constraint imposed by  $\theta_{\max}$ , that is,

$$\begin{aligned} & \min_{\boldsymbol{\theta}} g(\boldsymbol{\theta}), \\ & \text{s.t. } |\theta[n]| < \theta_{\max}, \end{aligned} \quad (12)$$

where  $g(\boldsymbol{\theta})$  measures the PSL as

$$g(\boldsymbol{\theta}) = \max_{\substack{m \neq 0 \\ \beta \neq 0}} \left( W[m, \beta] \cdot \frac{|\psi_{\text{WAF}}[m, \beta]|}{\max |\psi_{\text{WAF}}[m, \beta]|} \right). \quad (13)$$

Here,  $\frac{|\psi_{\text{WAF}}[m, \beta]|}{\max |\psi_{\text{WAF}}[m, \beta]|}$  is the normalized WAF, and  $W[m, \beta]$  is a weighting function that adjusts sensitivity to delay and Doppler shifts. For instance, higher weights can be assigned to lower delays and Doppler shifts to achieve greater sensitivity. In this work, we will use

$$W[m, \beta] = \frac{1}{1 + m^2 + \beta^2}. \quad (14)$$

Alternatively, a window in the delay-Doppler domain can be designed to optimize the PSL over any desired region of the delay-Doppler plane,  $\varpi$ . Then, the optimization problem in (12) can be modified as

$$\begin{aligned} & \min_{\boldsymbol{\theta}, Q} Q, \\ & \text{s.t. } W[m, \beta] \cdot \frac{|\psi_{\text{WAF}}[m, \beta]|}{\max |\Psi_{\text{WAF}}[m, \beta]|} \leq Q, \quad (m, \beta) \in \varpi, \\ & \quad |\theta[n]| < \theta_{\max}, \end{aligned} \quad (15)$$

where  $Q$  is an auxiliary variable representing the value related to the PSL.

Since Equation (15) (or (12)) is highly nonlinear with many

local minima, we solve it using particle swarm optimization (PSO). PSO is attractive for IUDC integration because of its simplicity, flexible constraint handling, robust global search, and low sensitivity to initial values [14]. Specifically, to solve (15), the algorithm begins by defining the position and velocity of the  $i$ th particle as

$$\mathbf{d}_i = [Q_i, \boldsymbol{\theta}_i]^T, \quad (16)$$

$$\mathbf{v}_i = [\Delta Q_i, \Delta \boldsymbol{\theta}_i]^T, \quad (17)$$

where  $i = 1, 2, \dots, N_p$ , and  $N_p$  denotes the particle swarm size (i.e., the number of particles). The variables  $Q_i$  and  $\boldsymbol{\theta}_i$  represent the target to be optimized for the  $i$ th particle. Equation (17) defines the particle velocity, where  $\Delta Q_i$  is a scalar velocity, and  $\Delta \boldsymbol{\theta}_i = [\Delta \theta_i[0], \Delta \theta_i[2], \dots, \Delta \theta_i[N-1]]^T$  is the phase velocity sequence. To ensure particles remain within the defined search space, velocities are constrained to a specified range. Consequently, the update equation for the  $i$ th particle is given by  $\mathbf{d}_i(t+1) = \mathbf{d}_i(t) + \mathbf{v}_i(t+1)$ , where

$$\mathbf{v}_i(t+1) = \omega \mathbf{v}_i(t) + \eta_1 r_1 (\mathbf{p}_{\text{best}} - \mathbf{d}_i(t)) + \eta_2 r_2 (\mathbf{g}_{\text{best}} - \mathbf{d}_i(t)). \quad (18)$$

Here,  $t$  represents the current iteration, and  $\eta_1$  and  $\eta_2$  are learning factors associated with the particle's personal best ( $\mathbf{p}_{\text{best}}$ ) and the global best ( $\mathbf{g}_{\text{best}}$ ), typically ranging from  $\eta_1 = 1.5$  to  $\eta_2 = 2.0$ . The random numbers  $r_1$  and  $r_2$  are introduced to enhance randomness and improve search diversity [15]. The inertia weight  $\omega$  plays a critical role in balancing global and local searches: a higher initial  $\omega$  (e.g., 0.8–1.0) promotes global exploration, while a lower  $\omega$  later in the iterations (e.g., 0.4–0.6) focuses on local search and convergence. It is common practice to dynamically adjust  $\omega$  as

$$\omega = \omega_{\max} - (\omega_{\max} - \omega_{\min}) \cdot \frac{t}{T}, \quad (19)$$

where  $T$  is the maximum number of iterations. By iterating over the  $N_p$  particles, each particle is evaluated using  $\mathbf{d}_i(t)$  and processed via (13) to yield  $g(\boldsymbol{\theta}_i)$ . The iterations continue until the difference between successive solutions is less than a threshold  $\epsilon$ . At convergence, the global optimum  $\mathbf{g}_{\text{best}}$  is obtained, yielding the optimal sequence  $\boldsymbol{\theta}[n], n = 0, \dots, N-1$ .

This sequence is then substituted into  $x'[n]$  and applied to (3) to generate the improved AFDM signal. This new PSO-optimized random perturbation P4 coding algorithm is called Optimized Random Perturbation P4 (ORP-P4) encoding. The specific ORP-P4 algorithm process is shown in Alg. 1.

For a point on the delay-Doppler plane  $(m, \beta)$ , the computational complexity of Equation (4) is  $O(N^3)$ . Assuming a single iteration, where  $T$  is the maximum number of iterations and  $N_p$  represents the number of particles (increasing with search granularity), the per-iteration complexity is  $O(TN_p)$ . Thus, the overall ORP-P4 algorithm complexity is  $O(TN_pN^3)$  [16].

---

**Algorithm 1** ORP-P4 Encoding Algorithm for AFDM Signal

---

**Input:** Communication symbol sequence  $\{x[n]\}$ , number of subcarriers  $N$ , system parameters  $c_1, c_2$ , maximum phase perturbation  $\theta_{\max}$ , swarm size  $N_p$ , maximum iterations  $T$ , learning factors  $\eta_1, \eta_2$ , inertia weight bounds  $\omega_{\max}, \omega_{\min}$

**Output:** Optimized AFDM signal  $s[k]$

- 1: Compute the P4 phase  $\phi[n]$ , for  $n = 0, \dots, N-1$ , according to Eq. (9).
  - 2: **Initialization:** For each particle  $i = 1, \dots, N_p$ , do:
    - Randomly generate an initial phase perturbation vector  $\boldsymbol{\theta}_i(0)$  satisfying  $|\boldsymbol{\theta}_i[n](0)| \leq \theta_{\max}$ .
    - Set the initial state  $\mathbf{d}_i(0) = [Q_i(0), \boldsymbol{\theta}_i(0)]^T$  and initial velocity  $\mathbf{v}_i(0)$ .
    - Evaluate the objective function  $g(\boldsymbol{\theta}_i(0))$  (which measures the WAF sidelobe level).
  - 3: Set each particle's best state:  $p_{\text{best}} = \mathbf{d}_i(0)$ , and set the global best:  $g_{\text{best}} = \arg \min\{g(\boldsymbol{\theta}_i(0))\}$ .
  - 4: **for**  $t = 0$  to  $T-1$  **do**
  - 5:   Update inertia weight: set  $\omega(t) = \omega_{\max} - (\omega_{\max} - \omega_{\min}) \frac{t}{T}$  (see Eq. (18)).
  - 6:   **for** each particle  $i = 1, \dots, N_p$  **do**
  - 7:     Update the velocity using Eq. (17): compute  $\mathbf{v}_i(t+1)$  by substituting  $\mathbf{v}_i(t)$ ,  $p_{\text{best}}$ ,  $g_{\text{best}}$ , and random factors  $r_1, r_2$ .
  - 8:     Update the state: compute  $\mathbf{d}_i(t+1) = \mathbf{d}_i(t) + \mathbf{v}_i(t+1)$ , and enforce the constraint  $|\boldsymbol{\theta}_i[n](t+1)| \leq \theta_{\max}$ .
  - 9:     Evaluate  $g(\boldsymbol{\theta}_i(t+1))$ .
  - 10:    **if**  $g(\boldsymbol{\theta}_i(t+1)) < g(p_{\text{best}})$  **then**
  - 11:     Set  $p_{\text{best}} = \mathbf{d}_i(t+1)$ .
  - 12:    **end if**
  - 13:   **end for**
  - 14:   Update the global best:  $g_{\text{best}} = \arg \min\{g(p_{\text{best}}) : i = 1, \dots, N_p\}$ .
  - 15:   **if** convergence criterion is met **then**
  - 16:     **break**
  - 17:   **end if**
  - 18: **end for**
  - 19: Let  $\boldsymbol{\theta}_{\text{opt}}$  be the phase perturbation vector from  $g_{\text{best}}$ .
  - 20: Compute the modified symbols:  
set  $x'[n] = x[n] \exp\{j(\phi[n] + \boldsymbol{\theta}_{\text{opt}}[n])\}$ .
  - 21: Generate the time-domain signal  $s[k]$  via IDAFT by substituting  $x'[n]$ ,  $c_1$ ,  $c_2$ , and  $N$  into Eq. (3).
  - 22: **return**  $s[k]$
- 

#### IV. SIMULATION RESULTS

In this section, we consider an AFDM signal with  $N = 128$  subcarriers and parameters  $c_1 = 2$  and  $c_2 = 1$ . The symbol duration is 10 ms, the bandwidth is  $B = 12.8$  kHz, and the carrier frequency is  $f_c = 5$  kHz. The radial velocity ranges from -10 to 10 m/s. All simulations consider  $N_p = 50$  particles and a maximum of  $T = 100$  iterations, with both individual and global learning factors set to  $\eta_1 = \eta_2 = 2.0$ . Unless stated otherwise, the maximum allowable phase is  $\theta_{\max} = \pi/4$ .

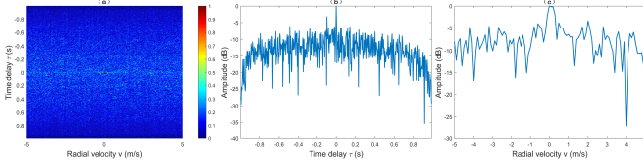


Fig. 3. WAF (a), zero radial velocity (b), and zero time delay (c) for a P4 encoded signal

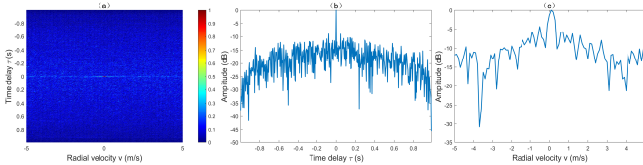


Fig. 4. WAF (a), zero radial velocity (b), and zero time delay (c) for the ORP-P4 encoded signal

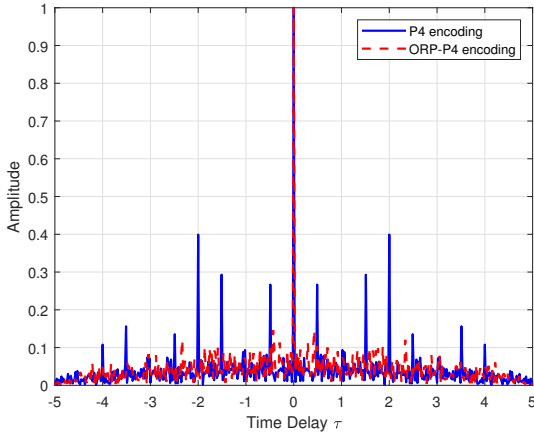


Fig. 5. Autocorrelation sequence for P4 and ORP-P4 signals

Figure 3 and Figure 4 show a comparison of the WAFs obtained using traditional P4 encoding and ORP-P4 encoding. In both cases, identical encoding information is employed, and the AFDM transmission signal serves as the carrier. Additionally, subfigures (b) and (c) in each figure display the WAF slices for zero radial velocity and zero time delay, respectively. It is evident that the proposed ORP-P4 algorithm produces a distinctive “thumbtack” WAF that decays rapidly in all directions, thereby enhancing the resolution of both radial velocity and time delay. Moreover, it reduces the interference observed outside the origin in traditional P4 encoding, mitigating the adverse effects of time delay and radial velocity on detection. These results demonstrate the superior performance of ORP-P4 in IUDC detection. Furthermore, Figure 5 illustrates that, compared to traditional P4 encoding, ORP-P4 encoding exhibits stronger autocorrelation and lower sidelobe levels.

Figure 6 compares the probability of detection,  $P_D$ , of various encoding methods using peak-to-average ratio detection at a probability of false alarm of  $P_F = 0.05$  and a signal length of one AFDM symbol (10 ms). Concretely, the detector

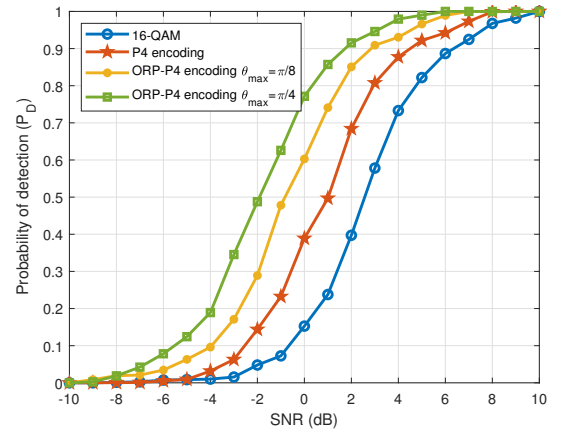


Fig. 6. Probability of detection for different coding methods

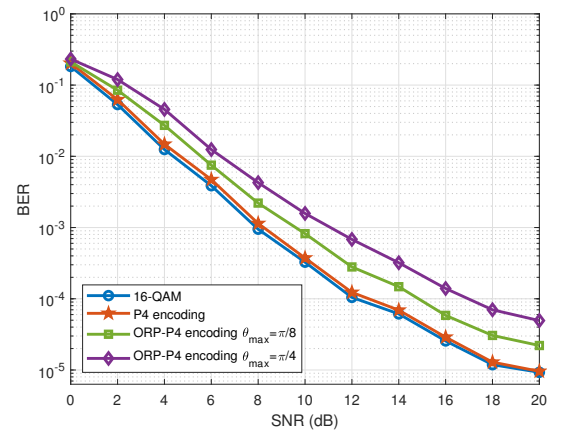


Fig. 7. BER comparison for different encoding methods

is based on the cross-correlation between the received and transmitted waveforms and uses as test statistic the ratio of the peak to the mean of the cross-correlation [17].

For each SNR level, the detection threshold is determined using Monte Carlo simulations. Specifically, in simulation experiments involving a target (characterized by radial velocity and delay, and incorporating a Jakes multipath channel), multiple independent transmissions are performed. For each trial, the peak-to-average ratio of the cross-correlation between the received and transmitted signals is calculated and compared to the preset false alarm probability to establish the detection threshold. The detection probability is defined as the ratio of the number of trials in which the target is detected to the total number of trials. As shown in Figure 6, the proposed ORP-P4 encoding demonstrates the best detection performance, especially for larger values of  $\theta_{\max}$ . Moreover, its performance surpasses that of both 16-QAM and the unoptimized P4 algorithm.

The communication performance of the proposed technique is also essential for evaluating the IUDC system. Figure 7 shows the bit error rate (BER) at different SNR levels. Under the same SNR conditions, the performance of standard P4 encoding is nearly identical to that of using 16-QAM alone.

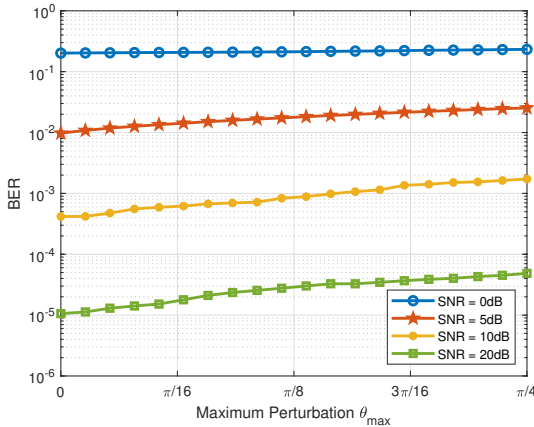


Fig. 8. BER comparison for varying  $\theta_{\max}$  and different SNRs

Although the proposed ORP-P4 algorithm enhances detection performance by optimizing the WAF through phase perturbation, the introduction of random perturbations—which can generally be regarded as noise—degrades its communication performance. Nevertheless, as the figure indicates, the BER remains acceptable in light of the significant improvements in detection performance.

In Figure 7, the BER performance of ORP-P4 for different values of  $\theta_{\max}$  is presented. To thoroughly examine the relationship between  $\theta_{\max}$ , SNR, and BER, Figure 8 was generated. As shown in the figure, as  $\theta_{\max}$  increases, the performance gradually deteriorates, which corroborates the results in Figure 7. These findings also provide valuable guidance for selecting an appropriate  $\theta_{\max}$  for the algorithm.

## V. CONCLUSION

This paper first models the underwater multipath channel and the transmitted signal based on the AFDM waveform, demonstrating that differences in the encoding method can affect the WAF. Therefore, a coding technique with stronger correlation is proposed to improve the detection performance of AFDM in IUDC systems. To this end, an improved P4 coding method for AFDM signals is presented, which employs phase perturbation optimized by the particle swarm optimization (PSO) algorithm to reduce the sidelobe level of the AWF, thereby enhancing detection performance. Simulation results indicate that this method effectively improves the peak-to-sidelobe ratio of the WAF, resulting in a "thumbtack-shaped" WAF and improved detection performance. Although the bit error rate increases slightly due to the receiver's inability to account for the random perturbation, the degradation is acceptable in view of the significant detection performance enhancement. Therefore, the trade-off between communication and detection performance makes the proposed technique highly suitable for integrated underwater detection and communication systems.

## ACKNOWLEDGMENT

This work was supported by the National Natural Science Foundation of China (NSFC) under Grant No. 62371393.

The work of D. Ramírez was partially supported by MCIU/AEI/10.13039/501100011033/FEDER, UE, under grant PID2021-123182OB-I00 (EPiCENTER), by the Office of Naval Research (ONR) Global under contract N62909-23-1-2002, by the Comunidad de Madrid under grant TEC-2024/COM-89 (IDEA-CM), and by the Spanish Ministry of Economic Affairs and Digital Transformation and the European Union-NextGenerationEU through the UNICO 5G I+D SORUS project.

## REFERENCES

- [1] A. Jahanmir, S. M. Majid Ashraf, R. Amin Khalil, and N. Saeed, "ISAC-enabled underwater IoT network localization: Overcoming asynchrony, mobility, and stratification issues," *IEEE Open Journal of the Communications Society*, vol. 5, pp. 3277–3288, 2024.
- [2] Y. Xiong, F. Dong, and F. Liu, "Information-theoretic limits of integrated sensing and communications," *Information-Theoretic Radar Signal Processing*, pp. 375–404, 2024.
- [3] Y. Ni, P. Yuan, Q. Huang, F. Liu, and Z. Wang, "An integrated sensing and communications system based on affine frequency division multiplexing," *IEEE Transactions on Wireless Communications*, pp. 1–1, 2025.
- [4] Y. Ni, Z. Wang, P. Yuan, and Q. Huang, "An AFDM-based integrated sensing and communications," in *International Symposium on Wireless Communication Systems*, 2022.
- [5] H. Hawkins, C. Xu, L.-L. Yang, and L. Hanzo, "IM-OFDM ISAC outperforms OFDM ISAC by combining multiple sensing observations," *IEEE Open Journal of Vehicular Technology*, vol. 5, pp. 312–329, 2024.
- [6] X. Zhao, W. Deng, M. Li, and M.-J. Zhao, "Robust beamforming design for integrated sensing and covert communication systems," *IEEE Wireless Communications Letters*, vol. 13, no. 9, pp. 2566–2570, 2024.
- [7] Y. He, G. Yu, and Y. Cai, "Rate-adaptive coding mechanism for semantic communications with multi-modal data," *IEEE Transactions on Communications*, vol. 72, no. 3, pp. 1385–1400, 2024.
- [8] F. Ihle, S. Lindner, and M. Menth, "P4-PSFP: P4-based per-stream filtering and policing for time-sensitive networking," *IEEE Transactions on Network and Service Management*, vol. 21, no. 5, pp. 5273–5290, 2024.
- [9] P. Braca, P. Willett, K. LePage, S. Marano, and V. Matta, "Bayesian tracking in underwater wireless sensor networks with port-starboard ambiguity," *IEEE Transactions on Signal Processing*, vol. 62, no. 7, pp. 1864–1878, 2014.
- [10] J. Yin, W. Men, X. Han, and L. Guo, "Integrated waveform for continuous active sonar detection and communication," *IET Radar, Sonar & Navigation*, vol. 14, no. 9, pp. 1382–1390, 2020.
- [11] A. F. Molisch, "Statistical description of the wireless channel," in *Wireless Communications*, 2011, pp. 69–99.
- [12] J. Zhu, Y. Tang, C. Yang, C. Zhang, H. Yin, J. Xiong, and Y. Chen, "A phase-coded time-domain interleaved OTFS waveform with improved ambiguity function," in *IEEE Globecom Workshops*, 2023.
- [13] R. Lin, M. Soitanalian, B. Tang, and J. Li, "Efficient design of binary sequences with low autocorrelation sidelobes," *IEEE Transactions on Signal Processing*, vol. 67, no. 24, pp. 6397–6410, 2019.
- [14] D. Wang, D. Tan, and L. Liu, "Particle swarm optimization algorithm: An overview," *Soft Computing*, vol. 22, no. 2, pp. 387–408, 2018.
- [15] A. G. Gad, "Particle swarm optimization algorithm and its applications: A systematic review," *Archives of Computational Methods in Engineering*, vol. 29, no. 5, pp. 2531–2561, 2022.
- [16] J. A. T. Machado, S. M. A. Pahnehkolaei, and A. Alfi, "Complex-order particle swarm optimization," *Communications in Nonlinear Science and Numerical Simulation*, vol. 92, p. 105448, 2021.
- [17] Q. Niu, Q. Zhang, and W. Shi, "Waveform design and signal processing method for integrated underwater detection and communication system," *IET Radar, Sonar & Navigation*, vol. 17, no. 4, pp. 617–627, 2023.